






Observation of topological edge states induced solely by non-Hermiticity in an acoustic crystalHe Gao ¹, Haoran Xue ^{2,*}, Qiang Wang,² Zhongming Gu ¹, Tuo Liu ¹, Jie Zhu,^{1,3,†} and Baile Zhang ^{2,4,‡}¹*Department of Mechanical Engineering, The Hong Kong Polytechnic University, Hung Hom, Kowloon, Hong Kong SAR, China*²*Division of Physics and Applied Physics, School of Physical and Mathematical Sciences, Nanyang Technological University, Singapore 637371, Singapore*³*The Hong Kong Polytechnic University Shenzhen Research Institute, Shenzhen 518057, China*⁴*Centre for Disruptive Photonic Technologies, Nanyang Technological University, Singapore, 637371, Singapore*

(Received 14 January 2020; revised manuscript received 5 March 2020; accepted 8 April 2020; published 6 May 2020)

Non-Hermiticity alters band topology in the presence of loss and/or gain in topological systems, which not only introduces new definitions in topological classifications, topological invariants, and the bulk-boundary correspondence, but also gives rise to unprecedented applications such as topological insulator lasers. Most existing non-Hermitian topological systems derive their topological phases from Hermitian components, rather than being driven by non-Hermiticity itself. Here we report on the experimental observation of topological edge states induced solely by non-Hermiticity in an acoustic crystal. The acoustic crystal consists of a periodic one-dimensional chain of coupled acoustic resonators with tunable loss. In the Hermitian limit, or when the loss is negligible, the crystal exhibits no band gap and hosts no topological edge states. By introducing loss, we show that a band gap is induced, which can be either topological or trivial, depending on the loss configuration. In the topological case, topological edge modes are found inside the band gap. These results demonstrate that non-Hermiticity is able to drive a topological phase transition from a trivial system to a topological one, offering the possibilities for actively steerable topological wave manipulations in applications ranging from acoustics to photonics.

DOI: [10.1103/PhysRevB.101.180303](https://doi.org/10.1103/PhysRevB.101.180303)

Introduction. Over the past decades, topological phases of matter have been systematically studied under the condition of Hermiticity [1–3]. A Hermitian system can be classified into the ten Altland-Zirnbauer symmetry classes according to internal symmetries [4], and is associated with real eigenenergies and orthogonal eigenstates, which give rise to well-defined topological invariants and bulk-boundary correspondence [5,6]. On the other hand, non-Hermiticity naturally arises in many cases, especially in classical wave systems where loss and/or gain are introduced intentionally or inevitably [7,8]. In such situations, non-Hermiticity significantly enriches topological phases beyond the Hermitian classification [9,10] and alters the bulk-boundary correspondence with unconventional modifications [11–17].

Various interesting phenomena have been observed. In particular, researchers have demonstrated the interaction between topological insulators and gain and loss, observing phenomena such as selective enhancement of topological edge states [18], parity-time-symmetric topological interface states [19], topological interface created by gain and loss [20], and lasing from topological boundary states [21–23]. More recently, observations of non-Hermitian skin effect and breakdown of conventional bulk-boundary correspondence have also been

reported [24–26]. Non-Hermiticity also alters the spectrum of topological semimetals significantly, splitting the band degeneracies into exceptional objects [27–29].

Most existing non-Hermitian topological systems derive their topological properties from Hermitian components. In other words, the systems are topological in the Hermitian limit and the non-Hermiticity generally brings in perturbations to the topological systems. On the other hand, recent theories have shown that non-Hermiticity can play a critical role rather than just bringing in perturbations. It has been proposed that non-Hermiticity can drive a topologically trivial system to undergo a topological phase transition and acquire topological properties [16,30–34]. This non-Hermiticity-induced topological phase transition opens a new direction for studying non-Hermitian topological physics and offers novel possibilities for active functional topological devices.

In this Rapid Communication we experimentally demonstrate non-Hermiticity-induced topological edge states in an acoustic crystal [35–39] with deliberately introduced loss [40]. Before the deliberate introduction of loss, the crystal is an array of coupled acoustic resonators with uniform on-site loss. It exhibits no band gap and hosts no topological edge states. When additional loss is deliberately introduced to two of every four resonators, a band gap is opened. This band gap can be either topological or trivial, depending on the loss

*haoran001@e.ntu.edu.sg

†jie.zhu@polyu.edu.hk

‡blzhang@ntu.edu.sg

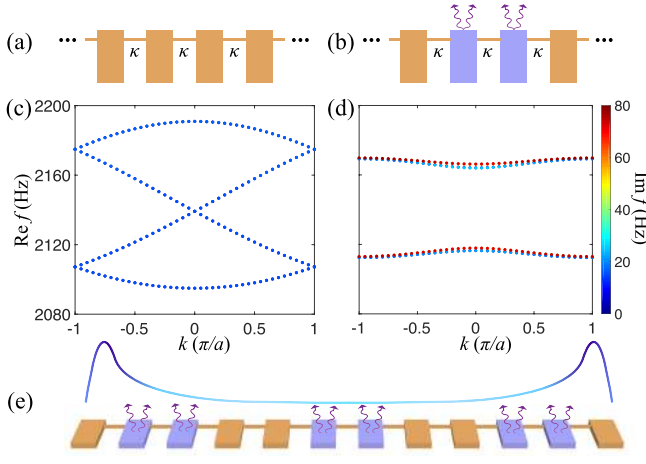


FIG. 1. (a) Schematic of a 1D acoustic crystal of coupled acoustic resonators with $\gamma_1 = \gamma_2 = 0$. A large cell containing four resonators is shown. (b) Schematic of a 1D acoustic crystal of coupled acoustic resonators with $\gamma_1 = \gamma_2 \neq 0$. Here one unit cell consists of four resonators. The resonators which are colored in blue have additional loss. (c) and (d) Corresponding dispersions of the lattices in (a) and (b), respectively. The color denotes the imaginary parts of the eigenfrequencies. (e) Schematic of the loss-induced topological edge states in a finite-sized crystal.

$$H(k) = \begin{pmatrix} (1 - i\gamma_0)f_0 & \kappa & 0 & \kappa e^{-ika} \\ \kappa & [1 - i(\gamma_0 + \frac{\gamma_1 + \gamma_2}{2})]f_0 & 0 & \kappa \\ 0 & \kappa & \kappa & 0 \\ \kappa e^{ika} & 0 & [1 - i(\gamma_0 + \gamma_1)]f_0 & [1 - i(\gamma_0 + \frac{\gamma_1 - \gamma_2}{2})]f_0 \end{pmatrix}, \quad (1)$$

where $a = 304\text{mm}$ is the lattice constant, κ is the coupling strength between resonators, f_0 is the resonance frequency, and γ_0 corresponds to the background loss which shifts the imaginary part of all the eigenfrequencies. The parameters $\gamma_{1,2}$ are used to describe the additionally introduced loss. γ_1 is the additional loss introduced to certain sites. γ_2 is a control parameter and only takes values of $\pm\gamma_1$, determining which two sites have additional loss. As can be seen from Eq. (1), when $\gamma_2 = \gamma_1$, the imaginary parts of on-site terms are $\{-i\gamma_0, -i(\gamma_0 + \gamma_1), -i(\gamma_0 + \gamma_1), -i\gamma_0\}f_0$, which indicates the central two sites have additional loss. When $\gamma_2 = -\gamma_1$, the imaginary parts of on-site terms are $\{-i\gamma_0, -i\gamma_0, -i(\gamma_0 + \gamma_1), -i(\gamma_0 + \gamma_1)\}f_0$, which indicates the right two sites have additional loss. This lattice can be regarded as a non-Hermitian version of Su-Schrieffer-Heeger (SSH) model [43], where the dimerized couplings are effectively replaced with gain and loss [31,32]. Different from adding gain and loss to the two sublattices of a standard SSH chain [18,19], here one unit cell consists of four sites instead of two, and the non-Hermiticity opens a band gap rather than narrows down the band gap. The nontrivial topology is captured by a biorthogonal polarization [15,32,34,44]

$$p^{\alpha\beta} = -\frac{1}{2\pi} \int_k^{k+\frac{2\pi}{a}} \text{Tr}[A^{\alpha\beta}(k)]dk, \quad (2)$$

configuration. In a nontrivial loss configuration, a topological band gap is observed with in-gap topological edge states. In a trivial loss configuration, instead, a trivial band gap is observed with no feature of any edge state.

Acoustic model. We start with a one-dimensional (1D) four-site unit cell as shown in Fig. 1(a), where each site is a hard-wall hollow acoustic resonator filled with air. Each resonator has dimensions of $80 \times 40 \times 10\text{mm}^3$. The resonators are coupled through thin hard-wall waveguides. The resonance mode of interest for these resonators is the dipole mode at 2136.3Hz [41]. Here we neglect the influence of other resonance modes [42]. There is a uniform background loss of $-i\gamma_0$ for each resonator due to the material absorption. The dispersion of this lattice is shown in Fig. 1(c), which is folded from that of one-site unit cell. It exhibits a trivial gapless band structure. Then we introduce additional loss to the two sites marked in blue in Fig. 1(b) [31]. Now each unit cell consists of four resonators and a band gap opens because of the additional loss [Fig. 1(d)]. As we will demonstrate in the following, this band gap is topologically nontrivial with topological edge states emerging at the edges of a finite sample [Fig. 1(e)].

Under single-mode approximation, the physics of this acoustic lattice can be described by a tight-binding model, whose k -space Hamiltonian is

where $[A^{\alpha\beta}(k)]_{mn} = -i\langle u_m^\alpha(k) | \partial_k | u_n^\beta(k) \rangle$ is the biorthogonal non-Abelian Berry connection. Here $\alpha, \beta = L, R$ denote left and right eigenvectors, and $m, n = 1, 2$ refer to the lower two bands. Due to the absence of exceptional points, the normalization $\langle u_m^\alpha(k) | u_n^\beta(k) \rangle = \delta_{mn}$ is satisfied for every k . In general, the biorthogonal polarizations defined in Eq. (2) are complex. Yet they satisfy $p^{LR} = (p^{RL})^*$ [34,44]. Thus, we can define a real-valued polarization as $p = (p^{LR} + p^{RL})/2$. With numerical eigenvectors obtained from finite element simulations [41], p is calculated to be 0.5 when $\gamma_1 = \gamma_2$ and 0 when $\gamma_1 = -\gamma_2$, which we refer to as the topological phase and the trivial phase, respectively.

The nontrivial bulk properties are linked to boundary observables in a finite-sized sample. First, we consider a 1D chain with 12 coupled resonators and with only background loss, as shown in Fig. 2(a). The simulated eigenmodes form a continuous spectrum. Then we introduce additional loss to the two central sites, which corresponds to the case $\gamma_1 = \gamma_2$ [see the inset to Fig. 2(b)]. A band gap is opened, in agreement with the bulk dispersion in Fig. 1(b). Moreover, inside the band gap there are two edge modes [see Fig. 2(d) for their profile] as the consequence of the nontrivial topology ($p = 0.5$). In contrast, if the additional loss is introduced to the right two sites in the unit cell ($\gamma_1 = -\gamma_2$), then p is 0 and no in-gap states are found [Fig. 2(c)].

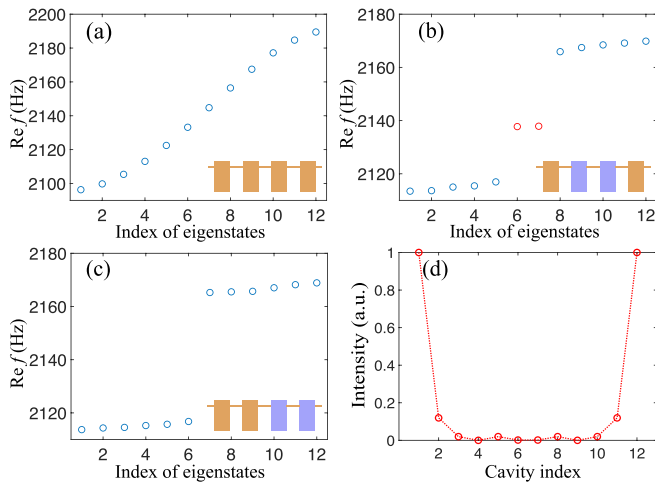


FIG. 2. (a)–(c) Simulated eigenfrequencies of a finite-sized acoustic crystal with $\gamma_1 = \gamma_2 = 0$ (a), $\gamma_1 = \gamma_2 \neq 0$ (b), and $\gamma_1 = -\gamma_2 \neq 0$ (c). Each finite-sized crystal consists of 12 resonators. (d) Sum of the amplitudes for the two in-gap states in (b).

Single resonator with additional loss. We now proceed to experimentally demonstrate the above phenomena. To do so, we first need to implement additional loss to a single resonator. We start with a single 3D-printed resonator with only background loss [see Fig. 3(a)]. There are two small holes ($r = 1$ mm) at two sides of the resonator, allowing for excitation and detection. The measured spectrum, as shown in Fig. 3(c), has a single peak with a finite bandwidth caused by the background loss. Then we introduce additional loss by drilling small holes on the resonator [see inset to Fig. 3(b)], which lead to sound leakage as well as resonance frequency shift. To minimize the frequency shift, absorbing materials are inserted into these holes (but not into the original cavity).

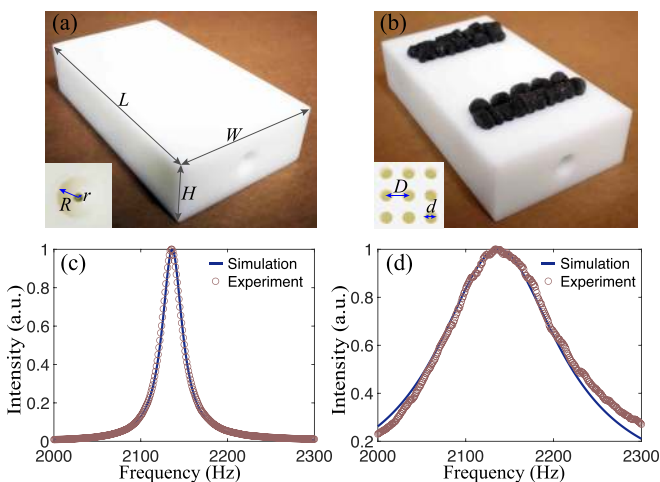


FIG. 3. (a) and (b) Photos of 3D printed single resonators with only background loss (a) and with additional loss (b). Values for the parameters are: $L = 92$ mm, $W = 52$ mm, $H = 22$ mm, $r = 1$ mm, $R = 4$ mm, $d = 2.4$ mm, $D = 4$ mm. The wall thickness is 6 mm. (c) and (d) Measured spectra (red dots) for the sample in (a) and (b), which are normalized to the peak value in respective spectrum. Blue solid lines are corresponding simulation results.

As a result, the measured spectra shows a single peak with a broader bandwidth. The estimated quality factor drops from 76 to 13 while the peak frequency almost remains the same [Fig. 3(d)]. We also fit numerical simulations to the experimental data here to obtain the effective loss parameter (as imaginary part of sound speed) used in all simulations [41].

Observation of non-Hermiticity-induced topological edge states. Having realized one single resonator with different losses, we now study the physics of 1D finite lattices. First, we fabricate a sample consisting of 12 coupled resonators with only background loss [Fig. 4(a)], corresponding to the gapless case in Fig. 2(a). We first measure the bulk spectrum by placing the speaker and microphone at the fifth and ninth resonators respectively as indicated in Fig. 4(a). As shown in Fig. 4(b), the spectrum is continuous, consistent with the simulation results in Fig. 2(a). Similar spectrum is obtained when both speaker and microphone are located at the first site [Fig. 4(c)]. Next, additional loss is introduced to the central two sites within each unit cell [Fig. 4(d)]. According to numerical results, now a topological band gap will open and edge states should be found. As shown is Fig. 4(e), in the bulk measurement two peaks are observed, indicating the existence of a band gap. In the edge measurement [Fig. 4(f)], one single peak is observed inside the band gap, which corresponds to the non-Hermiticity-induced topological edge mode. In contrast, when the additional loss is introduced to the right two sites within the unit cell [Fig. 4(g)], the system is still gapped [Fig. 4(h)]. However, there is no evidence of any in-gap state [Fig. 4(i)], since now this gap is topologically trivial. These observed results match well with numerical simulations. Details for the simulations and experimental setups can be found in [41].

Conclusion. In summary, we have observed topological edge states induced solely by non-Hermiticity. This is achieved in an acoustic crystal that consists of coupled acoustic resonators. The non-Hermiticity is introduced by creating additional absorption channels. We start with a gapless system with only background loss. Then additional loss is introduced to open a band gap, which is either topological or trivial depending on the loss configuration. Experimental measurement is performed for both nontrivial and trivial loss configurations, confirming the topological band gap with in-gap topological edge states in the topological case.

Our results reveal the rich interplay between non-Hermiticity and topology. Especially, rather than relying on the Hermitian part to acquire topological properties, non-Hermiticity itself suffices to drive a topological phase transition and induce nontrivial topology. This points to great potential applications since non-Hermiticity can be modulated externally, reconfigurably and actively. Our platform is potentially extendable to two dimensions and realize other non-Hermiticity-induced phenomena, such as higher-order topological states [32], Landau levels [33], and reciprocal skin effect [45]. Besides, the design here is based on a tight-binding model. Increasing the coupling strength and the additional loss, or extension beyond the tight-binding model will yield a larger band gap. It is also desirable to extend this idea from acoustics to photonics, where the topological edge states can serve as a reconfigurable high Q cavity for applications such as lasing.

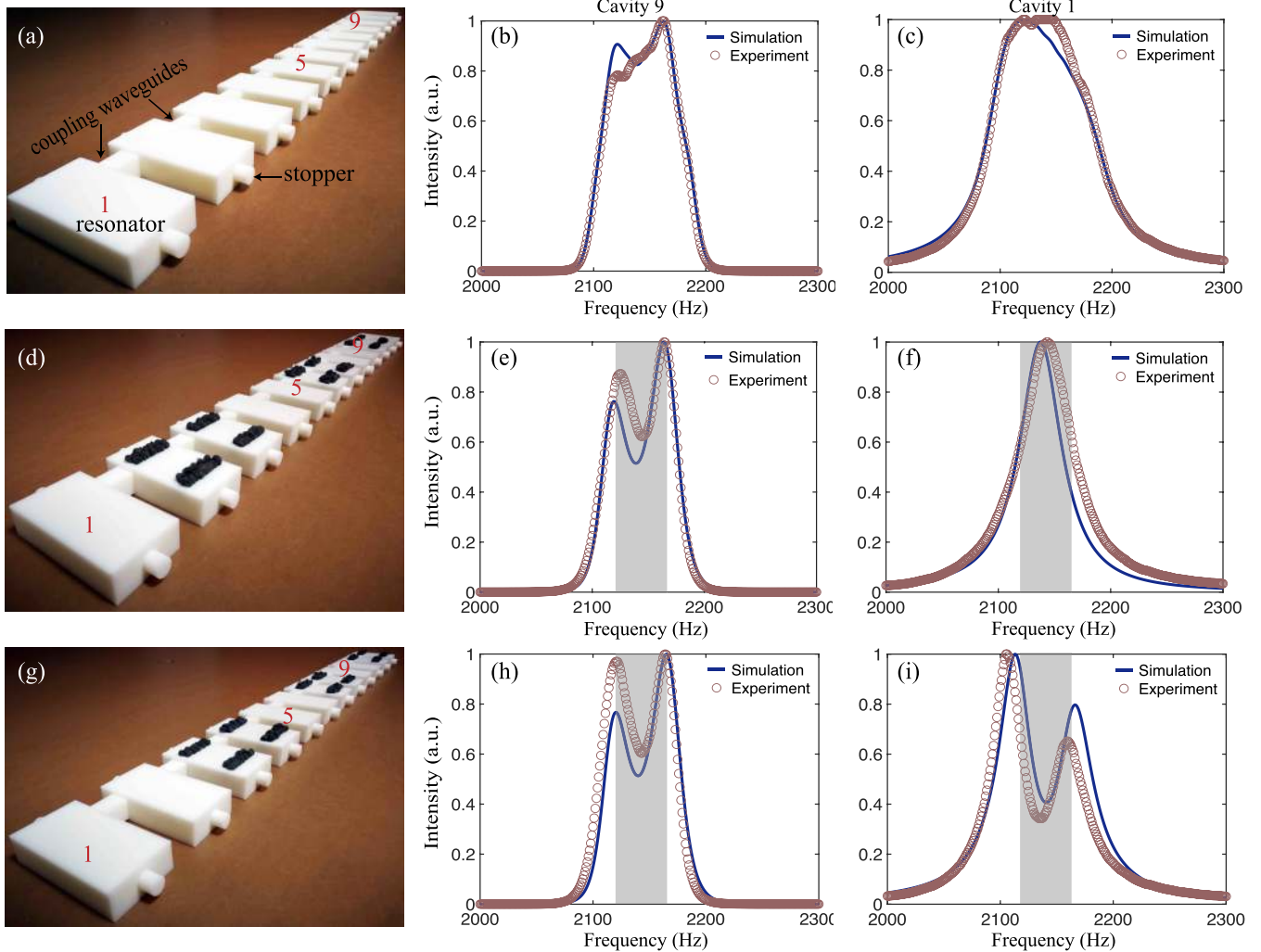


FIG. 4. (a) Photo of the 3D printed coupled acoustic resonator chain with $\gamma_1 = \gamma_2 = 0$. (b) Measured bulk spectrum for the sample shown in (a). (c) Measured edge spectrum for the sample shown in (a). (d)–(i) Similar to (a)–(c) but with $\gamma_1 = \gamma_2 \neq 0$ [(d)–(f)] and with $\gamma_1 = -\gamma_2 \neq 0$ [(g)–(i)]. In the bulk measurement, a speaker and a microphone are respectively placed at the fifth and the ninth resonator to observe the bulk transmission. In the edge measurement, both the speaker and the microphone are placed at the first resonator. In the spectrum plots, red dots are measured from experiments and solid blue lines are obtained from simulations, which are respectively normalized. In the simulations, the loss is considered as imaginary part of sound speed, whose values are determined from single resonator measurements [41].

Note added in proof. Recently, we became aware of a paper by Liu *et al.* [46] where topological phases are induced by non-Hermiticity in electrical circuit.

Acknowledgments. This research/project is supported by the Ministry of Education, Singapore, under its Tier 2 Award No. MOE 2018-T2-1-022(S). J.Z. acknowledges support from the General Research Fund scheme of Research Grants Council of Hong Kong under Grant No. PolyU 152119/18E.

- [1] M. Z. Hasan and C. L. Kane, *Rev. Mod. Phys.* **82**, 3045 (2010).
- [2] X.-L. Qi and S.-C. Zhang, *Rev. Mod. Phys.* **83**, 1057 (2011).
- [3] A. Bansil, H. Lin, and T. Das, *Rev. Mod. Phys.* **88**, 021004 (2016).
- [4] A. Altland and M. R. Zirnbauer, *Phys. Rev. B* **55**, 1142 (1997).
- [5] D. J. Thouless, M. Kohmoto, M. P. Nightingale, and M. den Nijs, *Phys. Rev. Lett.* **49**, 405 (1982).
- [6] J. Zak, *Phys. Rev. Lett.* **62**, 2747 (1989).
- [7] L. Feng, R. El-Ganainy, and L. Ge, *Nat. Photon.* **11**, 752 (2017).
- [8] R. El-Ganainy, K. G. Makris, M. Khajavikhan, Z. H.

- Muslimani, S. Rotter, and D. N. Christodoulides, *Nat. Phys.* **14**, 11 (2018).
- [9] K. Kawabata, K. Shiozaki, M. Ueda, and M. Sato, *Phys. Rev. X* **9**, 041015 (2019).
- [10] H. Zhou and J. Y. Lee, *Phys. Rev. B* **99**, 235112 (2019).
- [11] T. E. Lee, *Phys. Rev. Lett.* **116**, 133903 (2016).
- [12] D. Leykam, K. Y. Bliokh, C. Huang, Y. D. Chong, and F. Nori, *Phys. Rev. Lett.* **118**, 040401 (2017).
- [13] H. Shen, B. Zhen, and L. Fu, *Phys. Rev. Lett.* **120**, 146402 (2018).

- [14] S. Yao and Z. Wang, *Phys. Rev. Lett.* **121**, 086803 (2018).
- [15] F. K. Kunst, E. Edvardsson, J. C. Budich, and E. J. Bergholtz, *Phys. Rev. Lett.* **121**, 026808 (2018).
- [16] Z. Gong, Y. Ashida, K. Kawabata, K. Takasan, S. Higashikawa, and M. Ueda, *Phys. Rev. X* **8**, 031079 (2018).
- [17] D. S. Borgnia, A. J. Kruchkov, and R.-J. Slager, *Phys. Rev. Lett.* **124**, 056802 (2020).
- [18] C. Poli, M. Bellec, U. Kuhl, F. Mortessagne, and H. Schomerus, *Nat. Commun.* **6**, 6710 (2015).
- [19] S. Weimann, M. Kremer, Y. Plotnik, Y. Lumer, S. Nolte, K. G. Makris, M. Segev, M. C. Rechtsman, and A. Szameit, *Nat. Mater.* **16**, 433 (2017).
- [20] H. Zhao, X. Qiao, T. Wu, B. Midya, S. Longhi, and L. Feng, *Science* **365**, 1163 (2019).
- [21] M. A. Bandres, S. Wittek, G. Harari, M. Parto, J. Ren, M. Segev, D. N. Christodoulides, and M. Khajavikhan, *Science* **359**, eaar4005 (2018).
- [22] B. Bahari, A. Ndao, F. Vallini, A. El Amili, Y. Fainman, and B. Kanté, *Science* **358**, 636 (2017).
- [23] P. St-Jean, V. Goblot, E. Galopin, A. Lemaître, T. Ozawa, L. Le Gratiet, I. Sagnes, J. Bloch, and A. Amo, *Nat. Photon.* **11**, 651 (2017).
- [24] T. Helbig, T. Hofmann, S. Imhof, M. Abdelghany, T. Kiessling, L. W. Molenkamp, C. H. Lee, A. Szameit, M. Greiter, and R. Thomale, *arXiv:1907.11562*.
- [25] A. Ghatak, M. Brandenbourger, J. van Wezel, and C. Coulais, *arXiv:1907.11619*.
- [26] L. Xiao, T. Deng, K. Wang, G. Zhu, Z. Wang, W. Yi, and P. Xue, *Nat. Phys.*, **1** (2020), doi: 10.1038/s41567-020-0836-6.
- [27] B. Zhen, C. W. Hsu, Y. Igarashi, L. Lu, I. Kaminer, A. Pick, S.-L. Chua, J. D. Joannopoulos, and M. Soljačić, *Nature (London)* **525**, 354 (2015).
- [28] H. Zhou, C. Peng, Y. Yoon, C. W. Hsu, K. A. Nelson, L. Fu, J. D. Joannopoulos, M. Soljačić, and B. Zhen, *Science* **359**, 1009 (2018).
- [29] A. Cerjan, S. Huang, M. Wang, K. P. Chen, Y. Chong, and M. C. Rechtsman, *Nat. Photon.* **13**, 623 (2019).
- [30] S. Malzard, C. Poli, and H. Schomerus, *Phys. Rev. Lett.* **115**, 200402 (2015).
- [31] K. Takata and M. Notomi, *Phys. Rev. Lett.* **121**, 213902 (2018).
- [32] X.-W. Luo and C. Zhang, *Phys. Rev. Lett.* **123**, 073601 (2019).
- [33] H. Xue, Q. Wang, B. Zhang, and Y. D. Chong, *arXiv:1912.10937*.
- [34] J. Hou, Y.-J. Wu, and C. Zhang, *arXiv:1910.14606*.
- [35] M. Xiao, G. Ma, Z. Yang, P. Sheng, Z. Zhang, and C. T. Chan, *Nat. Phys.* **11**, 240 (2015).
- [36] H. Xue, Y. Yang, F. Gao, Y. Chong, and B. Zhang, *Nat. Mater.* **18**, 108 (2019).
- [37] H. Xue, Y. Yang, G. Liu, F. Gao, Y. Chong, and B. Zhang, *Phys. Rev. Lett.* **122**, 244301 (2019).
- [38] X. Ni, M. Weiner, A. Alù, and A. B. Khanikaev, *Nat. Mater.* **18**, 113 (2019).
- [39] L. Quan, D. L. Sounas, and A. Alù, *Phys. Rev. Lett.* **123**, 064301 (2019).
- [40] K. Ding, G. Ma, M. Xiao, Z. Q. Zhang, and C. T. Chan, *Phys. Rev. X* **6**, 021007 (2016).
- [41] See Supplemental Material at <http://link.aps.org/supplemental/10.1103/PhysRevB.101.180303> for more discussion on the mode shapes of single cavities, robustness of the bandstructure and details for simulations and experiments.
- [42] H. Xue, Y. Ge, H.-X. Sun, Q. Wang, D. Jia, Y.-J. Guan, S.-Q. Yuan, Y. Chong, and B. Zhang, *arXiv:1911.06068*.
- [43] W. P. Su, J. R. Schrieffer, and A. J. Heeger, *Phys. Rev. Lett.* **42**, 1698 (1979).
- [44] C. Yuce and H. Ramezani, *Phys. Rev. A* **100**, 032102 (2019).
- [45] T. Hofmann, T. Helbig, F. Schindler, N. Salgo, M. Brzezińska, M. Greiter, T. Kiessling, D. Wolf, A. Vollhardt, A. Kabaši *et al.*, *arXiv:1908.02759*.
- [46] S. Liu, S. Ma, C. Yang, L. Zhang, W. Gao, Y. J. Xiang, T. J. Cui, and S. Zhang, *Phys. Rev. Appl.* **13**, 014047 (2020).